ORIGINAL PAPER

Rheological properties and UV photo-oxidation of montmorillonite-filled random propylene–ethylene copolymers

Verónica Riechert[1,2] · Aníbal Ferrofino[1] · Lidia M. Quinzani[1] · Marcelo D. Failla[1,3]

Abstract

Random propylene–ethylene copolymers (RPC) are a type of polyolefin in increasing demand, mainly for packaging, due to its high impact resistance, large durability as well as high transparency and flexibility. The present study aims to investigate the morphological and rheological properties, as well as the photo-oxidation by UV irradiation, of five different RPCs and their nanocomposites. Organophilic montmorillonite is used as filler and maleic anhydride grafted RPCs as compatibilizers. Aging was performed by exposing strips of materials to UVA radiation for a maximum period of 96 h, and material degradation was analyzed following the evolution of carbonyl and hydroperoxide groups by FTIR and crystallinity by DSC. All nanocomposites display intercalated-exfoliated structure being the largest particle disaggregation presented by the polymer with the largest molecular weight. Rheological results support these observations. Neither the chemical composition of the polymers nor the presence of nanoclay/compatibilizer affects the photo-degradation mechanism of copolymers although the composite structure promotes the matrix photo-degradation. A parabolic relation was found between carbonyl and hydroxyl indexes of all stabilized and extracted materials, with or without clay. An increase in crystallinity with UV radiation dose was observed in all systems with a maximum determined in the case of the extracted systems.

Keywords Propylene–ethylene copolymers · Nanocomposites · Clay · Rheological properties · Photo-oxidation

✉ Marcelo D. Failla
mfailla@plapiqui.edu.ar

1   Planta Piloto de Ingeniería Química (PLAPIQUI), UNS-CONICET, Camino La Carrindanga Km 7, 8000 Bahía Blanca, Argentina

2   Departamento de Ingeniería Química, Universidad Nacional del Sur (UNS), Av. Alem 1253, 8000 Bahía Blanca, Argentina

3   Departamento de Ingeniería, UNS, Av. Alem 1253, 8000 Bahía Blanca, Argentina

Introduction

Random copolymers of propylene and α-olefins having low concentration of co-monomers (usually up to 10 wt%), RPC, have a wide range of applications in packaging, automotive and consumers goods [1]. The presence of co-monomer units gives place to materials that, in general, have higher impact resistance and lower softening temperature than propylene homopolymer (PP), with better transparency and flexibility. The most frequently used co-monomer to produce RPC is ethylene. 1-butene is also employed, and combined with ethylene produces propylene–ethylene–1-butene copolymers. The type and amount of co-monomer in RPC affect the final properties, basically by affecting the crystalline structure of the materials [2–4].

The range of applications of polyolefins can be extended using several strategies, like functionalization with polar groups and/or blending with other polymers or fillers [5–7]. In particular, layered silicates are frequently used to generate nanocomposites (NCs) since they have the potential to improve their physicochemical properties [7, 8]. Among these silicates, montmorillonite (MMT) is the most used nano-filler due to its large surface-to-volume ratio and high intercalation/exfoliation and cation exchange capacities [9]. This last characteristic of MMT is used to increase its compatibility with polyolefins by exchanging the inorganic cations present in its interlayer space with alkyl-cations. The so obtained organophilic MMT (oMMT) not only has improved organophilic character but also larger interlayer spacing than the original one, which facilitates the future exfoliation in tactoids and platelets and the intercalation of macromolecules.

Reinforcement of polyolefins with small amounts of oMMT is a known method to enhance properties like mechanical, thermal and barrier, maintaining the transparency and density of the original polymers [9]. However, in most cases, a functionalized polymer must be added to improve compatibility between polymer and clay in order to obtain well-dispersed and exfoliated nanoparticles. The presence of a small concentration of delaminated MMT increases the linear viscoelastic properties, mainly at low frequencies, of polyolefin NCs, being the rheological properties very sensitive to clay distribution [8, 10]. With respect to the crystalline structure of polyolefins, no clear trend of the effect of nanoparticles can be deduced from the results in the literature [11–13], while an improvement of their thermal stability and barrier properties is in general observed, depending on type and concentration of oMMT and compatibilizer [13–16].

During weathering of polyolefins, the most important phenomena is photo-oxidation, a process that requires oxygen and UV radiation in a range below 400 nm. Several studies, and even reviews, analyze the degradability of polyolefins and their composites and NCs [17–32]. Chemical changes are produced in polyolefins when subjected to UV irradiation in the presence of oxygen due to photo-oxidation. Chain scission and cross-linking, which takes place mainly in the amorphous region, can occur along with the formation of peroxides and different types of carbonyl compounds. The dominating reaction in the case of PP,

which is very rich in tertiary carbons, is chain scission that gives place to a notable reduction in molecular weight, mainly during the early stages of degradation, and significant decline of mechanical strength [17, 26]. PP and most PEs exhibit an increase in crystallinity during weathering at low UV radiation dosage. This is a consequence of chain scission and the phenomena called chemi-crystallization, which is promoted by the increasing chain mobility of shorter polymer segments that then can be integrated to crystalline phase [17, 26, 27, 30–32]. Additionally, a decreasing melting temperature is generally observed in PP and HDPE [27, 30–33], which is attributed to a rise in surface energy of crystallites, reduction in crystal thickness and incorporation of defects during crystallization.

Several authors have analyzed the effect of adding maleic anhydride (MA) grafted polyolefins and/or MMT to photo-oxidation of polyolefins. With respect to the effect of functionalized polymers, there is no agreement between observations. Some authors have detected an acceleration of the photo-degradation [21, 23], while others have found no specific effect [19, 20, 25]. Addition of MMT or oMMT to PP and PE gives place to microcomposites that, in general, photo-degrade earlier than their matrices, but not as much as when both compatibilizer and clay are added forming NCs [19–25, 27, 28]. The most notorious consequence of the presence of the filler is the decrease in induction time, which is the shortest in NCs. Authors associate the acceleration in photo-oxidation of polyolefin–clay systems to the combined effect of degradation of alkyl-ammonium cations present in oMMT, interaction of the polar groups in the clay with the generated carbonyl groups, and catalytic effect of impurities present in the clay, like Fe^{+2} and Ni^{+3}. The possible interaction between clay and stabilizer, when present, is another reason given to explain the reduction in induction time by lowering the efficiency of the protective additives.

In the present work, the effect of oMMT on rheological properties and UV degradation of RPC is studied. The very few references that may be found in the literature about this type of nanocomposites (N-RPC) mainly consider thermal [13, 34, 35], mechanical [34, 36], and rheological and barrier properties [37, 38]. No publication has been found that contemplates weathering behavior of RPC and their composites. In previous studies, we have analyzed the thermal and rheological properties of four different propylene–ethylene copolymers and propylene–ethylene-1-butene copolymer [4] as well as those of NCs based on the terpolymer [13, 38]. In the present work, the morphology, lineal viscoelastic behavior and UV photo-degradation of NCs of the copolymers are investigated. N-RPCs are prepared using 5 wt% of oMMT and 15 wt% of MA grafted RPCs. This work is motivated by the growing applications of RPC in packaging, automotive and agricultural industries, which demand improvement in the performance of this material and understanding of processing properties and stability to UV radiation to control its lifetime. Moreover, it is interesting to analyze the role that clay has on all these properties.

Experimental

Materials

The clay used in this work is *Nanomer I.44P* from *Nanocor* that has a particle size range of 15–25 μm. The organic modifier of this nanoclay is dimethyl dihydrogenated tallow ammonium chloride (2M2HTA). The polymers were provided by *PetroCuyo S.A.I.C.* Table 1 displays their identification code (ID) as well as co-monomer content, weight-average weight molecular weight (M_w) and polydispersity (PD) determined from size exclusion chromatography [4]. All RPC contain 3–4 wt% of ethylene, being T3 the only one that also has 8 wt% of 1-butene. Although the composition of the stabilizing system was not revealed by the producer, it was informed that C4 is the one with the largest stabilizer concentration.

MA grafted RPC (RPCg) were prepared by reactive melt mixing in a *Brabender Plastograph* mixer. 3 wt% of MA and 0.2 wt% of 2,5-dimethyl-2,5-di(tert-butyl peroxy) hexane were used. Details of processing and characterization of the functionalized polymers may be found in Riechert et al. [4] where the efficiency of grafting reaction is analyzed. Table 1 resumes the values of M_w, PD and anhydride group (AG) concentration of these polymers.

Composites were synthesized in the batch mixer by melt mixing the components during 20 min at 40 rpm and 160 °C under nitrogen atmosphere. RPC nanocomposites (N-RPC) were prepared using 5 wt% of oMMT and 15 wt% of the corresponding RPCg, which is added to improve compatibility between polymer and clay. Table 2 lists their ID code and composition. The material named C-T3, which is a composite based in T3 and 5 wt% of oMMT, without compatibilizer, is also part of the present study. A small amount, 0.01 wt%, of antioxidant *Irganox 1010* was added to all materials processed in the mixer.

Characterization

Infrared (FTIR) spectra of polymers and composites were obtained using a *Nicolet FTIR 520* spectrometer to characterize their chemical structure and to follow the changes after grafting and UV treatment. Transmission spectra were recorded in the range 4000–400 cm^{-1} with a resolution of 2 cm^{-1} from about 100-μm films obtained by compression molding.

Scanning electron microscopy (SEM) was employed to analyze phase structure of composite materials using a *LEO EVO-40 XVP* system. The analyzed surfaces were obtained with a cryo-ultra-microtome from specimens used in rheological characterization, that is, samples that have been subjected to 180 °C during a period of ~ 1 h in nitrogen atmosphere under minimum flow. The surfaces were chemically treated to enhance contrast between oMMT and polymer using a technique previously described [13].

X-ray diffraction (XRD) was applied to determine the interlayer spacing between stacked clay platelets in composite materials. The study was performed using a *Philips 3170* diffractometer equipped with a CuKa radiation source operated at

Table 1 Commercial and modified polymers used in the study

RPC						RPCg				
ID	Co-monomer content		M_w (kg mol^{-1})	PD	η_0 (Pa s)	ID	M_w (kg mol^{-1})	PD	AG grafted (wt%)	η_0 (Pa s)
	Ethylene	1-Butene								
C3l	3	–	161	1.9	1100	C3lg	95	1.7	0.88	210
C3m	3	–	195	2.3	2300	C3mg	110	2.0	0.72	300
C3h	3	–	347	2.9	3×10^4	C3hg	168	2.8	0.35	1400
C4	4	–	466	3.3	$\sim 3\times10^5$	C4g	152	2.0	0.52	1300
T3	3	8	225	2.2	5100	T3g	150	2.2	0.44	780

Their identification code (ID), weight-average molecular weight (M_w), polydispersity (PD), anhydride group content (AG) and zero-shear-rate viscosity (η_0) are listed

Table 2 Synthesized composites

| ID	Composition (wt%)			d_{001} (nm)
	RPC	RPCg	oMMT	
N-C3l	80	15	5	3.3
N-C3m	80	15	5	3.4
N-C3h	80	15	5	3.3
N-C4	80	15	5	3.4
N-T3	80	15	5	3.3
C-T3	95	–	5	3.3

Their identification code, composition and XRD clay basal spacing are listed

40 kV and 20 mA using a Ni filter. Diffraction spectra were recorded in the reflection mode over a 2θ range of 2–40° in steps of 0.02° using a rate of 0.6°/min. Diffractograms were collected from 150- to 200-μm thick films prepared by compression molding at 180 °C.

The elastic (G') and viscous moduli (G'') of all materials were measured in a rotational rheometer (*AR-G2, TA Instruments*) applying small amplitude oscillatory shear flow between parallel plates at 180ºC under nitrogen atmosphere. Disks of 25-mm diameter and 1.5-mm thick were cut from specimens previously molded using a hydraulic press. Dynamic frequency sweeps were performed within the linear viscoelastic region of each material under constant stress amplitude. The stress amplitude is selected from dynamic stress sweeps at 10 s^{-1}.

UV irradiation tests were performed using an *Accelerated QUV Weathering tester* (*Q-lab Corp.*) equipped with fluorescent UVA lamps. The tests were executed following the *ASTM G154* standard, exposing compression molded 0.2-mm thick strips to eight consecutive cycles. Each cycle involves 8 h of UVA irradiation at the black panel temperature of 60 °C followed by 4 h of vapor–water condensation at 50 °C without radiation. The irradiation intensity was 0.83 W m^{-2} at the wavelength of 340 nm. RPC specimens used to prepare the strips were previously processed in the mixer using the conditions listed for the composites. Tests were carried out also on samples previously treated by Soxhlet extraction during 16 h for stabilizer removal. Methyl-ethyl-ketone at boiling temperature was used for this procedure. Extracted materials are identified by adding a subscript "S" to their ID code. For example, T3$_S$ is a sample of T3 that has been subjected to solvent extraction. Specimens of extracted and non-extracted materials were taken from the camera at the end of each cycle for characterization. The oxidation occurring in the polymer during UV irradiation was assessed by FTIR. The heat of fusion and melting temperature of fresh and treated samples were also measured using differential scanning calorimetry (DSC) with a *PerkinElmer Pyris I* calorimeter. The thermograms were recorded in the range 30–170 °C applying a heating rate of 10 °C/min under nitrogen atmosphere.

Fig. 1 IR normalized spectra regions of the original (thin gray lines with solid circles), processed (thick black lines) and Soxhlet-extracted (thin black lines) RPC. Each set of spectra have been arbitrarily shifted along the y-axis
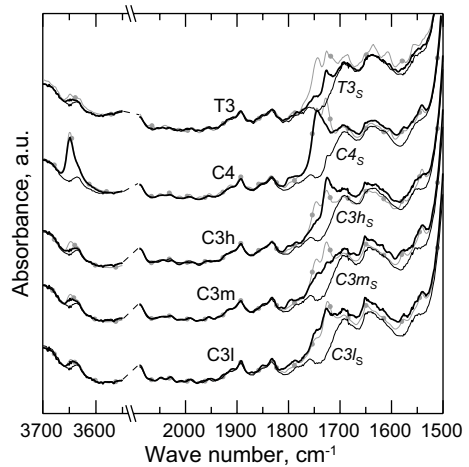
Results and Discussion

Infrared characterization of polymers and composites

Figure 1 displays the spectra of all polymers in the 1500–2100 and 3550–3700 cm^{-1} regions. The spectra of the original polymers (as provided by the producer), the RPC processed in the mixer and the solvent extracted materials are included. They have been normalized with the absorption band corresponding to the stretching of the methine group, at 2720 cm^{-1}. The larger difference among the spectra of original polymers appears in the absorption bands centered at 1720–1740 cm^{-1} and that at 3650 cm^{-1}, which can be associated with carbonyl and phenol groups of antioxidant, respectively. The location and intensity of these bands suggest that there exist differences in concentration and composition in the stabilizers used by the producer. As expected, both phenolic and carbonyl absorption bands are practically unnoticeable in the extracted polymers. In all RPC, the 3650 cm^{-1} band decreases from original to processed materials. This reveals that the mixing process, even with the addition of 0.01 wt% of *Irganox 1010*, consumes an important fraction of antioxidant. In fact, the intensities of the bands in the carbonyl region change after processing showing that the distribution of carbonyls groups is altered. Moreover, the lack of carbonyl absorption bands in the extracted materials suggest that polymers do not suffer noticeable oxidation during processing and that the carbonyl groups present in the processed RPC have to belong to the stabilizer. In agreement with the information given by the producer, C4 is the RPC with the largest concentration of stabilizer.

The IR spectra of processed RPC are presented once again in Fig. 2, together with those of grafted polymers (RPCg) and the corresponding NCs (N-RPC). The selected regions cover the ranges 1500–2100 and 3500–3750 cm^{-1}. The stretching of the OH groups of MMT produces an absorption band at 3637 cm^{-1} that can be appreciated in all composites. The band has a similar intensity in all spectra, agreeing with the fact that all composites were prepared with the same clay
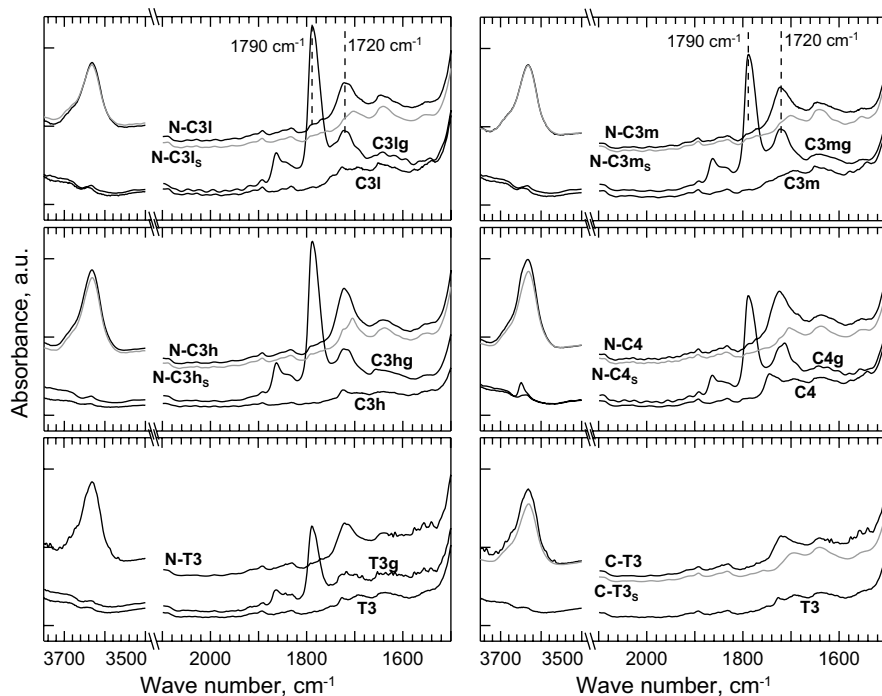
Fig. 2 Portions of IR spectra of all polymers and composites. The spectra have been arbitrarily shifted along the *y*-axis

concentration. However, they are not exactly equal, which may be related to alterations of the environment of the OH groups due to the state of intercalation/exfoliation of the clay [39]. In fact, it is interesting to observe that the peak intensity in the five NCs gradually increases in correspondence with the molecular weight of the copolymer. As it will be discussed later, the degree of exfoliation of the clay in the NCs also improves with molecular weight.

The 1500–2100 cm^{-1} region of the spectra includes the absorption bands associated to carbonyl groups. All RPCgs display an important band centered at 1790 cm^{-1} attributed to carbonyls of anhydride. This band does not appear in the corresponding copolymer spectra. RPCgs also present a series of overlapping bands centered at 1710–1730 cm^{-1} corresponding to carboxyl groups. These groups are mainly due to partial hydrolysis of AGs and secondary products of the grafting reaction [4]. The absorption band at 1790 cm^{-1} was used to calculate the concentration AGs in the grafted copolymers that are listed in Table 1. The amount of AG grafted into RPC depends on the stabilizer present, which reduces the efficiency of the reaction, and the chemical composition of the polymer. Given the small concentration of MA and peroxide used in the grafting reactions, the experimental uncertainty is another factor that must be considered. More information about the calculations is presented in Riechert et al. [4].

The analysis of N-RPC spectra show that the band at 1790 cm^{-1} present in RPCgs is practically undistinguishable in the composites, while that at 1720 cm^{-1} is more noticeable. The reactions that occur between the AGs of RPCg and the surfactant of oMMT are the cause of these behaviors, as it has been already discussed in the bibliography [13, 40]. Included in Fig. 2 are also the spectra of the solvent extracted N-RPC. In this case, the band at 1720 cm^{-1} practically disappears implying that most species with carbonyls are removed during treatment, including the added stabilizer.

Figure 2 also displays the spectrum of C-T3, the composite prepared without compatibilizer, and that of the corresponding extracted material, C-T3$_S$. C-T3 displays absorptions bands at about 1720 cm^{-1}, not present in C-T3$_S$, associated to the antioxidant. Compared to the location at which the carbonyl band corresponding to the stabilizer normally appears, at 1720–1740 cm^{-1} as already discussed, the band in C-T3 emerges slightly shifted toward lower wavenumbers. The interaction of antioxidant with chemical groups of the clay or its surfactant may be the cause of the observed shift [21].

Morphological characterization

The morphology of all composites was characterized by SEM. Figure 3 shows micrographs obtained with a magnification of 1000× of ultra-microtome cuts. This small magnification allows having a general vision of the microstructures and the degree of homogeneity of the distribution of clay in the polymeric matrices. The images are representative of the microstructure observed in all specimens of each material. The polymers appear as a dark background of the off-whiter clay particles. All specimens display homogeneous distribution of small particles and tactoids. However, N-C3l and N-C3m, the NCs prepared with the lower molecular weight polymers (see Table 1), and C-T3, the composite without compatibilizer,
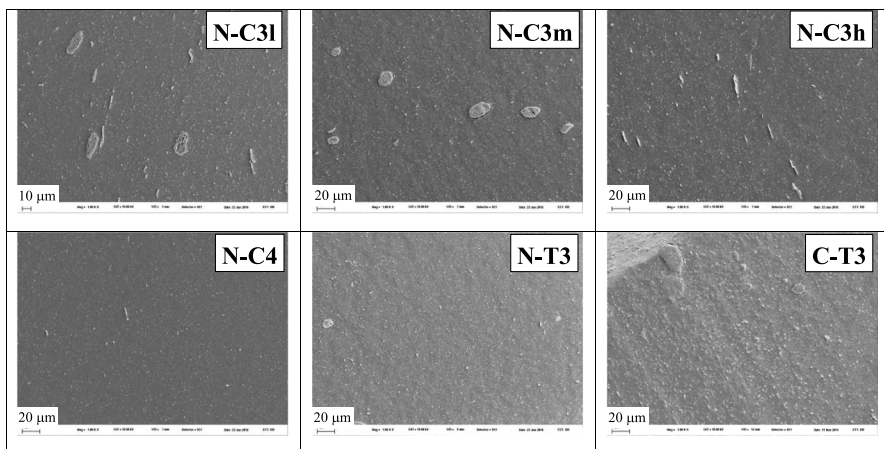

Fig. 3 SEM micrographs of composites taken with ×1000 magnification. Visualized areas: 317×225 μm

also display some large aggregates and original clay particles (~20 μm). N-C3h and N-T3 exhibit some aggregates of smaller size, while N-C4, which has been prepared with the higher molecular weight polymer, is the only NC that displays just very small tactoids. Practically, no aggregates appear in this material. As expected, the higher the molecular weight of the polymeric matrix, the better the degree of disaggregation of the clay, which is due to the high shear stresses generated during processing [38, 41].

Figure 4 displays micrographs taken at a magnification of 10,000× showing surfaces of all composites. Regardless of the presence of aggregates, all N-RPC display very small clay tactoids well-distributed in the polymeric matrices. Their maximum size is about 2 μm, which is in the order of MMT platelet diameter and much smaller than the ~20 μm average diameter of the original particles. The observed morphologies agree with the typical exfoliated structure found in compatibilized polypropylene NCs based on oMMT modified with 2M2HTA [15]. Nanoclay appears in the form of larger and more rigid particles in the case of C-T3 as it was previously
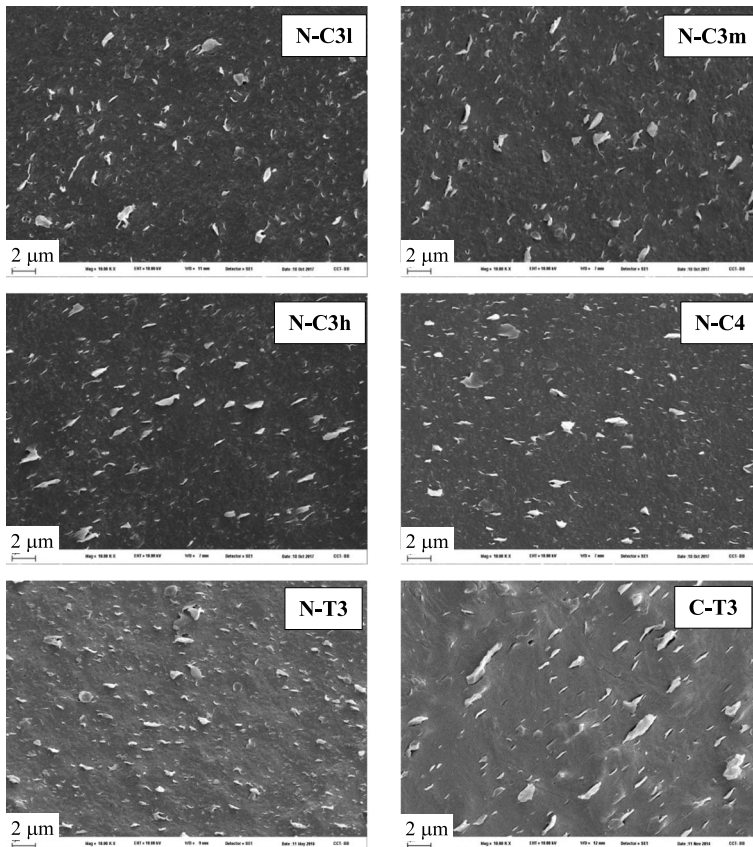

Fig. 4 SEM micrographs of composites taken with a magnification of ×10,000. Visualized areas: 31.7×22.5 μm

discussed [13]. As expected, the presence of a fraction of maleated polyolefin plays an important role in generated exfoliated composites [7].

XRD analysis allows the calculation of clay d_{001} basal spacing in the NCs by using Bragg's law. As shown in Table 2, values of 3.3–3.4 nm are obtained, which are larger than the 2.6 nm basal spacing of the original oMMT. The diffractogram of all NCs are similar to that of N-T3, which appears in Riechert et al. [13, 38] in comparison with that of C-T3. This similarity can be expected since all NCs are based in 5 wt% of clay and present similar size of tactoids as deduced from SEM. The combination of XRD results with those from SEM analysis determines that all N-RPC have intercalated partially exfoliated structure. C-T3 also displays a basal spacing of 3.3 nm, which means that the tactoids in this composite have an intercalated structure comparable to those of the NCs. This result was already discussed in Riechert et al. [13].

Rheological characterization

Figure 5 displays the elastic modulus (G') and the dynamic viscosity ($\eta' = G''/\omega$) of all polymers and composites. The data were obtained performing frequency sweeps at 180 °C. All RPC behave as homogeneous and simple polymers with properties that are in concordance with its molecular weight and PD (see Table 2). The Newtonian plateau can be clearly appreciated in the viscosity curves of C3l, C3m and T3, the RPC of lower molecular weight. Table 2 includes the zero-shear-rate viscosity ($\eta_0 = \eta'$ at $\omega \rightarrow 0$) of all polymers. These data were extracted from Riechert et al. [4] where a detailed study of the polymers and their blends with RPCgs is presented. According to the results discussed in that publication, all 80:15 blends of RPC/RPCg are miscible ones with rheological data that present a slight positive deviation with respect to a linear mixing rule. In fact, the dynamic data of the blends are not far from those of the original polymers. As an example, Fig. 5 shows the data
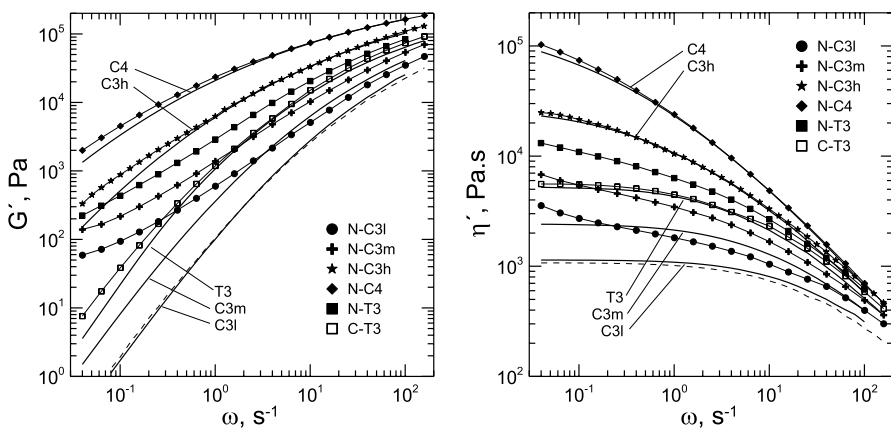

Fig. 5 Elastic moduli (G') and dynamic viscosity (η') of polymers and composites as a function of frequency at 180 °C. Solid lines: data of RPC. Dashed lines: data of the 80:15 blend of C3l and C3lg (equivalent to the matrix of N-C3l)

of C3l/C3lg blend, which is equivalent to N-C3l matrix. The data of this blend are presented with dashed lines that fall practically coincident with C3l moduli.

Most of the dynamic moduli of the NCs, on the other hand, fall far from those of the polymers, mainly in the case of low molecular weight RPCs. At high frequencies ($\omega > 10$ s^{-1}), where the system dynamics is dominated by the behavior of the polymers, the moduli of NCs approach those of their matrices. As the frequency descends, the moduli of each NC increase with respect to those of the corresponding polymer and RPC/RPCg blend. In fact, the difference becomes larger as ω decreases, mainly in the case of G'. For example, the ratio G'_{NC}/G'_{blend} at 0.04 s^{-1} takes values of 200, 50, 47, 2.5 and 1.5 for C3l, C3m, T3, C3h and C4, respectively. As it is well-known, the low-frequency region is the one most affected by the interactions between particles. The observed rheological behavior is typical of exfoliated NCs [9, 15] and is in agreement with the phase structures already analyzed. The interaction between nanoparticles is a slow relaxation process that consequently affect mainly the elasticity of materials at low frequencies. This process adds to the dynamic of macromolecules, which have larger relaxation time and moduli as the molecular weight increases. For this reason, the effect of the nano-filler is relatively less notorious in the polymers of higher molecular weight where the large moduli of the polymers mask the effect of interactions between nanoparticles [8, 10]. N-C4, with its very well exfoliated structure, is a good example that illustrates this comment. Liu and coworkers [37] studied a NC based on a copolymer similar to C3h using 2 wt% of oMMT. The rheological behavior of that system is in concordance with the results present in this paper. Figure 5 also displays the dynamic data of C-T3, the noncompatibilized composite. This material exhibits a behavior very different to that of N-T3. In fact, the moduli of C-T3 are not far from those of the polymer, T3. This is the typical behavior of microcomposites where the effect of the presence of a low concentration of clay particles is weak [8, 13].

The linear viscoelastic behavior of the materials can also be analyzed through tan δ ($= G''/G'$), which allows to analyze the relative importance of viscous behavior

Fig. 6 Phase angle (as tan δ) of polymers and composites as a function of frequency at 180 °C
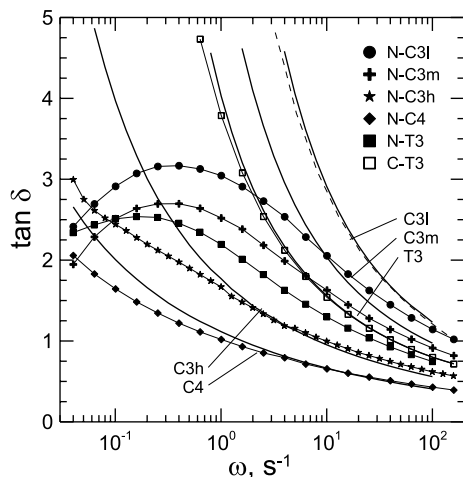
with respect to the elastic one. Figure 6 displays tan δ at 180 °C as a function of frequency of all polymers and composites. This way of presenting the data emphasizes that the relative increase produced by the presence of nano-filler in G' is larger than in G'' in all systems, since tan δ is always larger in the polymers than in the composites. As expected, the effect is more notorious in the low molecular weight polymers and at low frequencies. The important difference in rheological behavior between C-T3 and N-T3 also becomes quite notorious in this way of presenting the data.

UV degradation

Strips based on processed polymers and composites have been subjected to UV irradiation according to the treatment described in the Experimental Section. As it has been described in the literature, photo-oxidation is expected to occur during UV irradiation. The oxidation process of PP and RPC follows a free radical mechanism with a kinetics that proceeds following induction and auto-acceleration stages [17, 18, 26, 29, 31]. Concisely, this mechanism involves initial macroradicals that react with oxygen to produce oxy-radicals, which then can extract hydrogen from other molecular segments forming hydroperoxides. Hydroperoxide groups then decompose in alkoxy and peroxy radicals that continue the degradation process generating different carbonyl species on the macromolecules and some chain scission. Accordingly, FTIR is the technique typically used to monitor chemical changes in treated specimens.
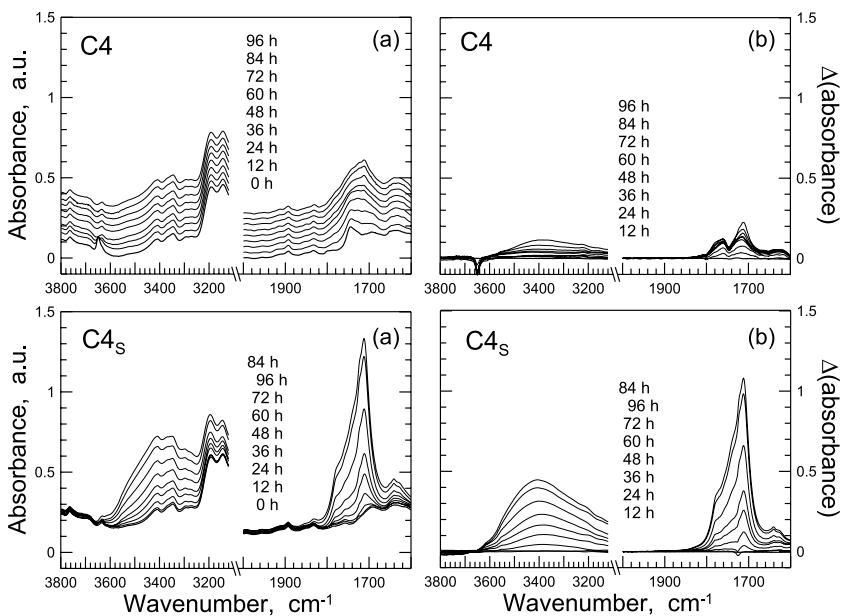

Fig. 7 **a** Evolution of IR spectra of C4 and C4$_S$ with time upon UV irradiation. **b** Difference between the spectra of treated films and that of the untreated material (0 h)

As already commented in the Experimental Section, the photo-degradation study includes a set of solvent extracted films. They are included to analyze the effect of the stabilizer added to prevent thermal oxidation but that also affects the photo-oxidative degradation of polymeric materials. To exemplify the behavior of the polymers with time of UV exposition, Fig. 7 displays IR spectra of C4 and C4$_S$. The spectra resulting from subtracting those of Fig. 7a to that of the non-irradiated material (0 h) are shown in Fig. 7b. Two wavenumber regions are shown: 1600–2000 and 3100–3800 cm^{-1}. The former includes the overlapping absorption bands centered at 1720–1740 cm^{-1} corresponding to carbonyls mainly from aldehyde, ketone, acid, ester and lactone groups [24, 31]. The high wavenumber region is where the bands associated with the stretching of hydroxyl groups from hydroperoxides, alcohols, carboxylic acids, etc., appear [24, 31]. The absorbance of both groups of bands increases with exposure time in both polymers, being the effect much notorious in the solvent-treated polymer, C4$_S$. In the high wavenumber region, a broad band at about 3400 cm^{-1} appears as photo-oxidation proceeds, pushing up the existing absorption bands in the polymers. This is clearly seen in Fig. 7b. Moreover, it can be observed that the maximum of the band gradually shifts toward higher wavenumbers with exposure time. This can be associated with a change in concentration of different OH groups as photo-degradation proceeds [18, 23, 31]. The gradual increase in absorbances with exposure time is interrupted in the case of C4$_S$, presenting the spectrum after 96 h of treatment lower absorbances than that of 84 h. This will be discussed further down when the degradation indices of all materials are presented. The larger intensity of carbonyl and hydroxyl bands reached by the Soxhlet-treated polymer is due to the lack of stabilizer in this material. As expected, the antioxidant added for thermal protection during processing also retards the photo-oxidative degradation of the polymers [19, 21, 25, 32].

Globally, as it will be discussed later, all RPC display a very low degradation rate up to ∼ 60–72 h, suggesting that the whole antioxidant package actually gradually loses its protective capacity during all this time. In fact, Fig. 7 shows that the spectra of C4 after 96 h of treatment are similar to those of C4$_S$ after 24–36 h, agreeing with the observation that the polymer has been protected during 60–72 h. As shown in Fig 1, C4 displays an absorption band at ∼ 3650 cm^{-1} corresponding to phenol groups of antioxidant. This band, which does not appear in C4$_S$, rapidly decreases in intensity during UV treatment, practically disappearing after 24 h. During that period, as the phenolic stabilizer gets consumed, the corresponding degradation products give place to an increase in carbonyl groups [42]. This early change was observed just in C4 (and it is fairly detected in C3m).

The time evolution of the IR spectra of nanocomposites N-C4 and N-C4$_S$ is shown in Fig. 8. Again, they exemplify the behavior displayed by all composites. The absorption band at 3640 cm^{-1} associated with OH groups of MMT is observed in all N-RPCs [20, 27]. This band does not change during UV treatment. The absorption bands associated with carbonyl and hydroxyls groups in both, N-C4 and N-C4$_S$, increase with time, being the Soxhlet-extracted composite the one that shows the largest absorbances. However, the increment is not gradual. Oscillations are detected, like in the case of 60-h spectrum of N-C4 that is above that of 72 h.
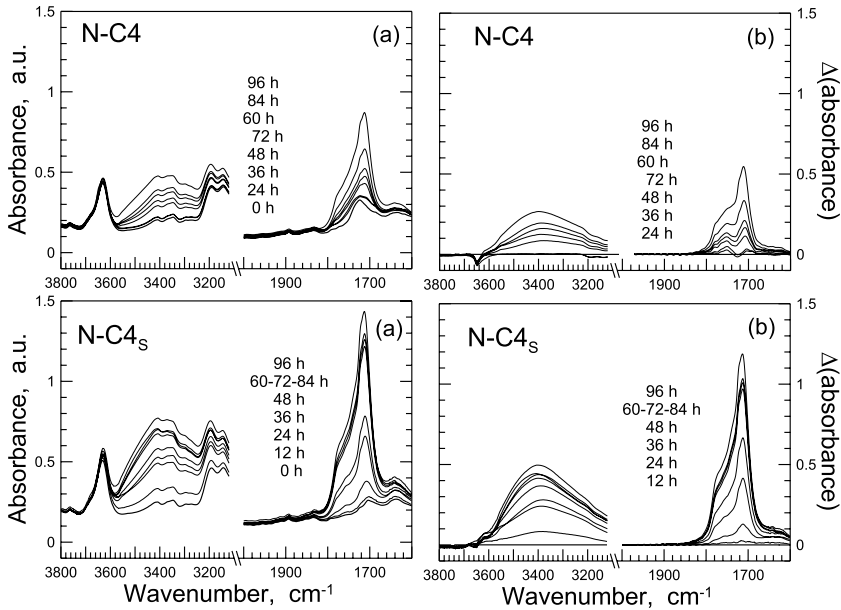
Fig. 8 **a** Evolution of IR spectra of N-C4 and N-C4$_S$ with time upon UV irradiation. **b** Difference between the spectra of treated films and that of the untreated material (0 h)

Similar oscillations occur in most composites at similar exposure times as will be commented further down.

The results already reported in the literature regarding photo-degradation of polyolefin NCs show that they degrade faster than the corresponding polymers. The analysis of photo-oxidation of NCs is complex because of the numerous factors to consider, like clay itself, alkyl-ammonium ions, clay impurities, air introduced to the mixer being trapped in the clay, compatibilizer, secondary products of reactions between compatibilizer and surfactant, amount and type of stabilizer, etc. [19–25, 27, 28]. None of them can be discarded. The discrimination of their influence would be a challenging work. In agreement with previous works, N-C4 shows faster photo-degradation than C4 (see Figs. 7a, 8a). For this to occur, reactions might be taking place that accelerate the consumption of the stabilizer inducing the early oxidation of the polymer, and/or the clay might be partially inhibiting the antioxidant activity and/or catalyzing the degradation. On the other hand, the comparison of N-C4 spectra with those of C4$_S$ indicates that even if nanoclay is inhibiting the action of the stabilizer, at least part of it is still acting since the photo-degradation rate of N-C4 is smaller than that of C4$_S$. Additionally, the difference between the spectra of C4$_S$ and N-C4$_S$ would suggest that the presence of organo-clay/compatibilizer slightly promotes photo-oxidation of the polymer since somewhat larger levels of degradation are reached for equivalent exposure time.

The area of the overlapping absorbance bands centered at 1720 cm^{-1}, covering the range 1670–1850 cm^{-1}, is used to define the carbonyl index (CI):

$$CI = \frac{A_{1670-1850} - A^0_{1670-1850}}{A_{2720}} \tag{1}$$

where $A^0_{1670-1850}$ is the corresponding area at 0 exposure time. Similarly, a hydroxyl index (HI) is defined using the area of the broad band in the 3150–3570 cm^{-1} range:

$$HI = \frac{A_{3150-3570} - A^0_{3150-3570}}{A_{2720}} \tag{2}$$

where $A^0_{3150-3570}$ is the area at 0 exposure time. Both, CI and HI, are calculated using as a reference the area of the band centered at 2720 cm^{-1}, which is not affected by photo-oxidation [17, 18].

Figure 9 displays the CI of all processed materials. Each value corresponds to an average of at least three measurements, which have a maximum dispersion of ± 12%. The original polymers display the lowest CI in the whole range of exposure time. In fact, the index departs from very small and practically constant values only after 60–72 h of treatment, when oxidation becomes noticeable. This period can be linked to the stabilizer loss of activity. Within this period, C4, and C3m in lower proportion, also show a clear augment of CI after the first two irradiation cycles. This behavior agrees with the decrease in concentration of the phenol groups associated with the stabilizer (absorption band at 3650 cm^{-1}). After 60–72 h, the antioxidant loses its protective capacity and polymers begin to photo-degrade faster. This is emphasized in the data of the solvent extracted materials, which display an oxidation induction time of ~24 h and reach much larger values of CI by the end of the process (96 h). In fact, the final CI is, in average, about five times larger in the
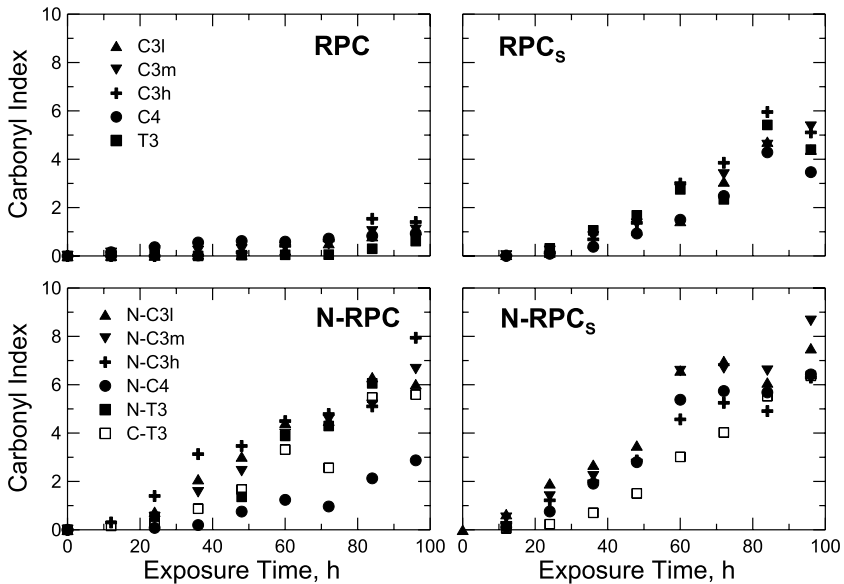

Fig. 9 Carbonyl index of all analyzed materials as a function of UV exposure time

solvent extracted polymers. The causes for the existence of an induction time in the solvent extracted materials are two. One is the irradiation time required for building up of hydroperoxides, before a noticeable concentration of carbonyl species can be detected [18]. The other reason that cannot be discarded is that, although not noticeable in Fig. 1, traces of stabilizer may still be present, beyond the detection limit of IR technique. La Mantia and Dintcheva [43] have suggested that it is possible to obtain generalized CI curves from stabilized and unstabilized PE by applying a shift factor, implying that the photo-oxidation mechanism is not altered by stabilizers. The data presented here may very well agree with that conclusion since, on average, the CI reached by the stabilized polymers after 96 h of treatment are practically coincident with those of the extracted polymers after ~ 36 h of treatment. The difference of about 60 h agrees with the time required by the stabilizer to lose its activity.

Once oxidation becomes evident, all polymers display similar oxidation rates with a practically linear behavior. The amount of ethylene and the presence of butylene in their composition seem not to affect the photo-degradation process of RPC. Globally, the results agree with those in the literature that analyze photo-degradation of PP under similar conditions of UV irradiation. Values of induction time up to 40 h have been reported with a practically linear increase of CI during ~ 100 h after stabilizer depletion [18, 23, 30, 33]. Both, induction time and rate of increase in CI depend on several factors, being the type and amount of antioxidant and the intensity of UVA irradiation the most important ones. It is interesting to observe that a change in trend appears at about 84 h in all solvent extracted materials. Oscillations in CI, which follow one another along an average increasing trend, have been observed by other authors while studying photo-oxidation of PP films [18, 29, 44]. Those studies suggest that during UV irradiation, there is an initial step with a quick increase in carbonyl group content caused by the rate controlled oxidation in the surface of the films. After that, photo-degradation continues with steps where oxygen diffusion competes with the faster oxygen consumption process as degradation goes deeper from the surface. Moreover, according to these authors, the appearance of microcracks on the sample surface, which would provide higher oxygen pressure inside the specimen, would make the CI oscillations more pronounced.

Figure 9 also displays the evolution of CI for the N-RPC. Globally, they show more degradation than the polymers at equivalent UV doses. An induction time of ~ 10 to 30 h can be appreciated that is followed by a practically linear increase in CI. After 96 h of exposure, the NCs reach a CI, that is, on average, seven times larger than the polymers, except in the case of N-C4 that displays a final CI that is just three times larger. In fact, N-C4 is the one with the longest induction time. The whole set of results of the N-RPC support, and even strengthen, the comments made when analyzing the C4 family of spectra showing that the presence of organo-filler/compatibilizer accelerates the photo-degradation of all polymers. In fact, the different package of stabilizer in the original C4 justifies the difference in behavior of N-C4 relative to the rest of NCs. The results shown in Fig. 9 suggest that the NCs of all RPC behave similarly to other polyolefins in regard to photo-oxidation degradation, with organo-clay/compatibilizer contributing to oxidation induced by UV exposure [19–25, 27, 28, 31, 45].

The comparison of CI of the solvent extracted polymers (RPC$_S$) and NCs (N-RPC$_S$) confirms the role of organo-filler/compatibilizer promoting the photo-degradation of polymers. In fact, RPC$_S$ present oxidation induction times of about 24 h and reach an average maximum CI of ~5, while N-RPC$_S$ present induction times shorter than 10 h and an average maximum CI of ~7. Moreover, C-T3$_S$, the microcomposite in which clay appears poorly delaminated, with less interaction surface, is the one that has the smaller values of CI. It is interesting to observe that the extracted NCs, like RPC$_S$, display a change in trend with exposure time. In this case, it appears at about 72 h.

When analyzing the composite data, it should be considered that processing itself may promote some degradation by the presence of oxygen adsorbed in the clay. Then, when materials are subjected to UV irradiation, photo-oxidation would initiate on samples that already have experienced some degradation and might contain a small amount of hydroperoxide groups, even if undetectable by IR technique. This may explain why both stabilized and extracted NCs display very similar induction times.

To further analyze the initial steps of photo-degradation of RPC, the hydroxyl index (HI) of all materials was also determined. Its value is plotted in Fig. 10 in relation to CI. The first result that can be drawn from this figure is that there is a remarkable agreement between the data of the different materials in each plot. Another interesting result is that, globally, the data of RPC$_S$ fall on a parabolic curve (see fitting included in the figure). Moreover, the indexes of stabilized polymers follow the same tendency reaching, as expected, lower values during the 96 h of UV exposure. At initial doses, HI increases faster than CI. In fact, the rate of carbonyl growth with
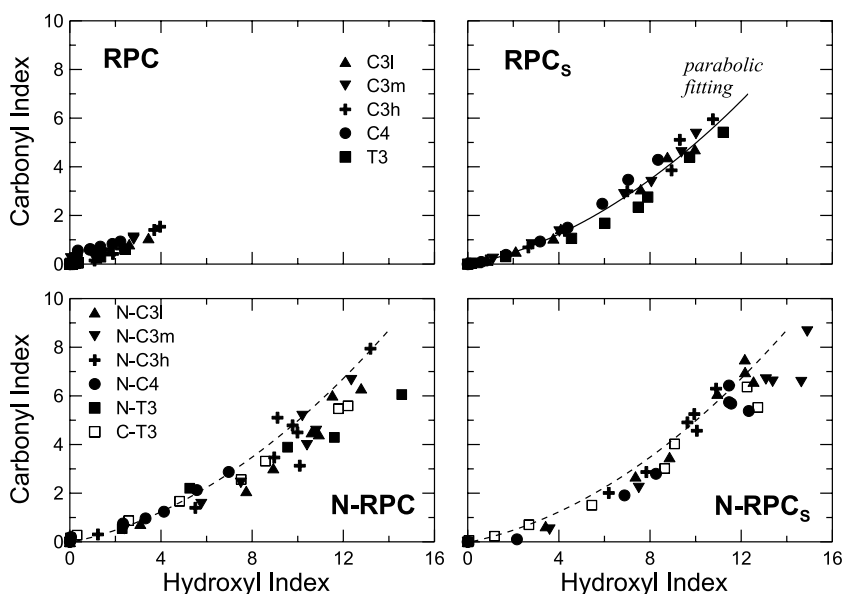

Fig. 10 Hydroxyl index as a function of carbonyl index for all materials. Dashed lines: replica of the parabolic fitting of RPC$_S$ data

respect to hydroperoxide (dCI/dHI) has a value of 0.25 at HI = 1 while at, for example, HI = 12 reaches a value of ~ 1. The initial low value is expected given the fact that, according to the photo-oxidation mechanism proposed for PP, the beginning of the process involves the buildup of hydroperoxides before different carbonyl groups appear in the macromolecules [29, 31].

Remarkably, all composites, micro- or nano-stabilized or not, display practically the same CI-HI behavior, with data that fall close to the parabolic fitting of the RPC$_S$ indexes (shown in dashed lines in N-RPC and N-RPC$_S$ data plots). This suggests that even if clay may be promoting the photo-degradation of the polymers, it does not affect the degradation mechanism itself. The presence of organo-clay/compatibilizer reduces the induction time allowing HI and CI to reach larger values in the 96 h of treatment. The observations above are in agreement with results of the literature that show that, once oxidation starts, the rate of increase in the degradation products is not affected by the presence of clay [19–21, 45].

Most of the samples used in the UV treatment were also characterized by measuring their degree of crystallinity (χ) from the fusion enthalpy (ΔH_m) as:

$$\chi = \frac{\Delta H_m}{\Delta H_m^0} \times 100 \tag{3}$$

where $\Delta H_m{}^0$ is the fusion enthalpy of 100% pure crystalline iPP with a value of 168 J g^{-1} [3]. In the case of composites, χ was calculated considering 95 wt% of polymeric mass. Table 3 lists the initial value of crystallinity (χ_0) and that after 96 h of UV treatment (χ_F) of all analyzed materials. Additionally, as an example of the evolution of χ along UV treatment, Fig. 11 displays the values of crystallinity of T3, C3h$_S$, N-T3 and N-C3h$_S$, which have been chosen as representative of the behavior of each group of materials.

As expected, χ_0 of the polymers is in concordance with their ethylene content, decreasing with co-monomer concentration [3, 4]. During treatment, crystallinity augments gradually up to final values that are about 22% larger than χ_0, following a

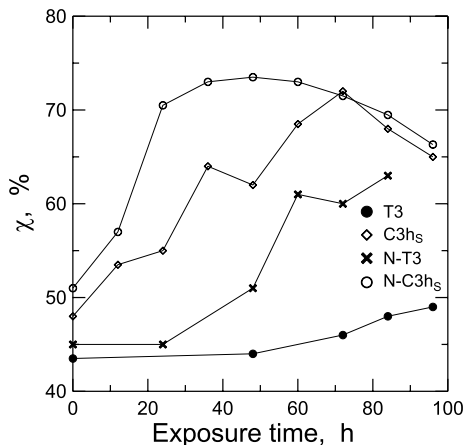**Fig. 11** Degree of crystallinity as a function of exposure time of representative materials

Table 3 Degree of crystallinity of samples before and at the end of UV treatment

RPC	χ_0 (%)	χ_F (%)	Relative increase (%)	Composite	χ_0 (%)	χ_F (%)	Relative increase (%)
C3l	51	62	22	N-C3l	50	76	52
C3m	49	59	20	N-C3m	52	77	48
C3h	48	59	22	N-C3h	51	75	47
C4	43	53	24	N-C4	45	62	38
T3	42	49	17	N-T3	42	63 (84 h)	50
				C-T3	42	72	71
C3l$_S$	52	64	23	N-C3l$_S$	59	64	9
C3m$_S$	52	61	17	N-C3m$_S$	56	64	14
C3h$_S$	53	65	23	N-C3h$_S$	57	65	14
C4$_S$	47	56	19	N-C4$_S$	49	62	26

The reported values correspond to the average from at least three runs, having standard deviations of up to 2%

trend similar to that observed in CI (see Fig. 9). Two phenomena contribute to the increment in crystallinity. On one side, the UV treatment involves an annealing process at 60 °C. This annealing at the temperature at which the fusion of the polymers begins [4] would allow the diffusion of small molecules and molecular segments toward the crystalline phase. The other phenomena is that of chemi-crystallization originated in the macromolecular scission occurring in the non-crystalline phase during photochemical degradation [17, 28, 30]. The larger mobility of short chain segments allows for their integration into the crystalline phase.

Table 3 also includes the crystallinity of the solvent extracted copolymers. These materials display initial and final crystallinity that are slightly larger than those of the original polymers. The larger values of χ_0 in the RPC$_S$ might be due to annealing occurring during stabilizer extraction. RPCs, however, display a significant increase in their crystallinity at the beginning of UV treatment going through a maximum at about 60–84 h. This behavior is exemplified in Fig. 11 for the case of C3h$_S$. The lack of stabilizer allows for a rapid increase in crystallinity since the beginning of UV exposure due to an important reduction in molecular weight [32]. The existence of a maximum followed by a decrease in χ can be justified by incorporation of defects in the molecular structure and interface degradation of crystallites [18, 32, 33].

As it has already been demonstrated, and it is shown in Table 3, the presence of 5 wt% of nanoclay does not noticeably affect the crystallinity of the polymers. On the other hand, after the UV treatment, the relative increase in crystallinity in the case of composites practically duplicates the value obtained in the polymers (~47% compared to 22%). This result, which is shown in Fig. 11 for N-T3, agrees with the increase in CI observed in the N-RPC when compared with the polymers. As it happens with the RPC$_S$, chemi-crystallization explains the observed behavior, which has already been seen by other authors when studying PP and PE nanocomposites [12, 27, 45].

With respect to the solvent extracted NCs, they display a global behavior similar to the extracted polymers. Their χ_0 is slightly larger than those of the N-RPC due to the annealing occurring during the extraction process, and they display a maximum crystallinity at about 24–72 h of exposure. The fact that the maximum occurs in earlier stages than in the RPCs agrees with the already concluded effect of nanoclay promoting photo-degradation of the polymers (Table 3).

Concluding remarks

Random propylene copolymer nanocomposites were prepared by melt mixing with 5 wt% organophilic montmorillonite and 15 wt% synthesized maleic anhydride grafted copolymers. Results from FTIR, SEM and XRD show that all compatibilized composites display intercalated partially exfoliated structure with homogeneous distribution of small tactoids. The larger the molecular weight of the polymeric matrix the better the degree of disaggregation observed in the clay. Accordingly, the dynamic moduli display a behavior typical of NCs with a remarkable increase, mainly of the elastic modulus at low frequencies, due to strong interactions between filler particles.

All copolymers display similar UV photo-oxidation behavior. The total exposure time considered was about one third larger than the average time required for the processing stabilizers added to the polymers to lose their protective action (60–72 h). The removal of stabilizers by solvent extraction produces a significant reduction in oxidation induction time with the corresponding increase in final level of degradation in the polymers. When the carbonyl index is analyzed as a function of hydroxyl index, a remarkable agreement was found between the data of all stabilized and extracted polymers. In fact, a parabolic relation was found between the indexes with a very small slope at initial doses.

Globally, NCs show larger degradation than the polymers at equivalent UV doses. The oxidation induction time is reduced by the presence of organo-clay/compatibilizer, which favors the photo-degradation of the copolymers. In fact, the oxidation induction time of solvent extracted polymers more than doubles that of extracted NCs. Remarkably, all composites, micro- or nano-stabilized or not, display practically the same CI-HI behavior, with data that fall close to the parabolic fitting of the RPC_S indexes. This suggests that even if clay may be promoting the photo-degradation of the polymers, it does not affect their degradation mechanism.

The chemi-crystallization that occurs during UV photo-degradation induces an increase in crystallinity of all materials which follows the evolution of the carbonyl index. The presence of clay promotes the photo-degradation of the polymers without affecting noticeably the crystallinity of the matrices. The lack of stabilizer allows for an initial rapid increase in crystallinity due to an important reduction in molecular weight. A maximum is then appreciated in this property generated by the competing processes of chemi-crystallization and incorporation of defects in the molecular structure and interface degradation of crystallites.

Declarations

Conflict of interest Not applicable.

References

1. Gahleitner M, Paulik C (2017) Polypropylene and other polyolefins. In: Gilbert M (ed) Brydson's plastics materials. Elsevier, Kidlington
2. Auriemma F, De Rosa C, Di Girolamo R, Malafronte A, Scoti M, Cioce C (2016) Molecular view of properties of random copolymers of isotactic polypropylene. In: Auriemma F, Alfonso GC, de Rosa C (eds) Polymer crystallization I. Springer, Berlin
3. Caveda S, Pérez E, Blázquez-Blázquez E, Peña B, van Grieken R, Suárez I, Benavente R (2017) Influence of structure on the properties of polypropylene copolymers and terpolymers. Polym Test 62:23–32
4. Riechert V, Ferrofino A, Ressia J, Failla MD, Quinzani LM (2019) Modification of propylene-α-olefin copolymers by maleic anhydride grafting and blending. Int J Polym Anal Charact 24:355–373
5. Moad G (1999) The synthesis of polyolefin graft copolymers by reactive extrusion. Prog Polym Sci 24:81–142
6. Karian H (2003) Handbook of polypropylene and polypropylene composites, 2nd edn. CRC Press, New York
7. Pandey JK, Reddy KR, Mohanty AK, Misra M (2014) Handbook of polymer nanocomposites. Processing, performance and application. Springer, Berlin
8. Utracki LA (2004) Clay-containing polymeric nanocomposites. Rapra Technology Limited, Shawbury
9. Sinha Ray S (2013) Clay-containing polymer nanocomposites: from fundamentals to real applications. Elsevier, London
10. Durmus A, Kaşgöz A, Macosko CW (2007) Linear low density polyethylene (LLDPE)/clay nanocomposites. Part I: Structural characterization and quantifying clay dispersion by melt rheology. Polymer 48:4492–4502
11. Morawiec J, Pawlak A, Slouf M, Galeski A, Piorkowska E, Krasnikowa N (2005) Preparation and properties of compatibilized LDPE/organo-modified montmorillonite nanocomposites. Europ Polym J 41:1115–1122
12. Dong Y, Bhattacharyya D (2010) Dual role of maleated polypropylene in processing and material characterization of polypropylene/clay nanocomposites. Mater Sci Eng A 527:1617–1622
13. Riechert V, Failla MD, Quinzani LM (2017) Effect of montmorillonite on the crystallization and thermal degradation of poly(propylene-co-ethylene-co-1-butene) nanocomposites. J Thermopl Comp Mater 30:741–761
14. Zhao C, Qin H, Gong F, Feng M, Zhang S, Yang M (2005) Mechanical, thermal and flammability properties of polyethylene/clay nanocomposites. Polym Degrad Stab 87:183–189
15. Rohlmann CO, Horst MF, Quinzani LM, Failla MD (2008) Comparative analysis of nanocomposites based on polypropylene and different montmorillonites. Eur Polym J 44:2749–2760
16. Lai SM, Chen WC, Zhu XS (2009) Melt mixed compatibilized polypropylene/clay nanocomposites. Part 1: The effect of compatibilizers on optical transmittance and mechanical properties. Compos A Appl Sci Manuf 40:754–765
17. Rabello MS, White JR (1997) Crystallization and melting behaviour of photodegraded polypropylene. 1 Chemi-crystallization. Polymer 38:6379–6387
18. Castejón ML, Tiemblo P, Gómez-Elvira JM (2000) Photo-oxidation of thick isotactic polypropylene films. I. Characterisation of the heterogeneous degradation kinetics. Polym Degrad Stab 70:357–364

19. Mailhot B, Morlat S, Gardette J-L, Boucard S, Duchet J, Gerard J-F (2003) Photodegradation of polypropylene nanocomposites. Polym Degrad Stab 82:163–167
20. Morlat-Therias S, Mailhot B, Gonzalez D, Gardette J-L (2004) Photooxidation of polypropylene/montmorillonite nanocomposites. 1 Influence of nanoclay and compatibilizing agent. Chem Mater 16:377–383
21. Morlat-Therias S, Mailhot B, Gonzalez D, Gardette J-L (2005) Photooxidation of polypropylene/montmorillonite nanocomposites. 2 Interactions with antioxidants. Chem Mater 17:1072–1078
22. Qin H, Zhang Z, Feng M, Cong F, Zhang S, Yang M (2004) The influence of interlayer cations on the photo-oxidative degradation of polyethylene/montmorillonite composites. J Polym Sci B Polym Phys 42:3006–3012
23. Qin H, Zhang S, Liu H, Xie S, Yang M, Shen D (2005) Photo-oxidative degradation of polypropylene/montmorillonite nanocomposites. Polymer 46:3149–3156
24. Kandilioti G, Elenis A, Macchiarola KA, Gregoriou VG (2006) Photooxidative degradation and conformational changes in syndiotactic polypropylene/clay nanocomposites. Appl Spectrosc 60:1285–1292
25. Dintcheva NTz, Al-Malaika S, La Mantia FP, (2009) Effect of extrusion and photo-oxidation on polyethylene/clay nanocomposites. Polym Degrad Stab 94:1571–1588
26. Rajakumar K, Sarasvathy V, Chelvan AT, Chitra R, Vijayakumar CT (2009) Natural weathering studies of polypropylene. J Polym Environ 17(3):191–202
27. Grigoriadou I, Paraskevopoulos KM, Chrissafis K, Pavlidou E, Stamkopoulos T-G, Bikiaris D (2011) Effect of different nanoparticles on HDPE UV stability. Polym Degrad Stab 96:151–163
28. Liu X, Gao C, Sangwan P, Yu L, Tong Z (2014) Accelerating the degradation of polyolefins through additives and blending (review). J Appl Polym Sci 131:40750
29. François-Heude A, Richaud E, Desnoux E, Colin X (2015) A general kinetic model for the photothermal oxidation of polypropylene. J Photochem Photobiol A Chem 296:48–65
30. Rouillon C, Bussiere P-O, Desnoux E, Collin S, Vial C, Therias S, Gardette J-L (2016) Is carbonyl index a quantitative probe to monitor polypropylene photodegradation? Polym Degrad Stab 128:200–208
31. Grause G, Chien M-F, Inoue C (2020) Changes during the weathering of polyolefins. Polym Degrad Stab 181:109634
32. Wu H, Zhao Y, Dong X, Su L, Wang K, Wang D (2021) Probing into the microstructural evolution of isotactic polypropylene during photo-oxidation degradation. Polym Degrad Stab 183:109434
33. Liu Q, Liu S, Xia L, Hu P, Lv Y, Liu J, Chen Z, Huang Y, Li G (2019) Effect of annealing-induced microstructure on the photo-oxidative degradation behavior of isotactic polypropylene. Polym Degrad Stab 162:180–195
34. Palza H (2010) Effect of co-monomer content on the behavior of propylene copolymer/compatibilizer/ clay nanocomposites. Macromol Mater Eng 295:492–501
35. Liu BB, Shangguan YG, Zheng QJ (2012) Toughening of ethylene-propylene random copolymer/clay nanocomposites: Comparison of different compatibilizers. Chin J Polym Sci 30:853–864
36. Prevosto D, Lucchesi M, Bertoldo M, Passaglia E, Ciardelli F, Rolla PJ (2010) Interfacial effects on the dynamics of ethylene–propylene copolymer nanocomposite with inorganic clays. Non-Cryst Solids 356:568–573
37. Liu BB, Shangguan YG, Song Y, Zheng QJ (2013) Influences of compatibilizers on rheology and mechanical properties of propylene random copolymer/styrene-ethylene-butylene-styrene block copolymer/organic-montmorillonite nanocomposites. Appl Polym Sci 129:973–982
38. Riechert V, Quinzani LM, Failla MD (2018) Linear viscoelasticity, extensional viscosity and oxygen permeability of nanocomposites based on propylene copolymer and organoclay. J Appl Polym Sci 135:45840
39. Madejová J, Pálková H, Komadel P, Yarwood J, Douthwaite R, Duckett SB (2010) IR spectroscopy of clay minerals and clay nanocomposites. Spectroscopic properties of inorganic and organometallic compounds: techniques. Mater Appl 41:22–71
40. Coiai S, Prevosto D, Bertoldo M, Conzatti L, Causin V, Pinzino C, Passaglia E (2013) Chemistry of interfacial interactions in a LDPE-based nanocomposite and their effect on the nanoscale hybrid assembling. Macromolecules 46:1563–1572
41. Gianelli W, Ferrara G, Camino G, Pellegatti G, Rosenthal J, Trombini RC (2005) Effect of matrix features on polypropylene layered silicate nanocomposites. Polymer 46:7037–7046

42. Reingruber E, Buchberger W (2010) Analysis of polyolefin stabilizers and their degradation products. J Sep Sci 33:3463–3475

43. La Mantia FP, Dintcheva NTz (2004) Photooxidation and stabilization of photooxidized polyethylene and of its monopolymer blends. J Appl Polym Sci 91:2244–2255

44. Girois S, Delprat P, Audouin L, Verdu J (1997) Oxidation thickness profiles during photooxidation of non-photostabilised polypropylene. Polym Degrad Stab 56:169–177

45. Salah HBH, Daly HB, Denault J, Perrin F (2016) UV degradation of clay-reinforced polypropylene nanocomposites. Polym Eng Sci 56:469–478